Draft version July 29, 2023
Typeset using LaTeX **twocolumn** style in AASTeX631

Improving the Distortion Solution for Brown Dwarf Parallax Measurements from the Canada-France-Hawaii Telescope

Abigail M. Colclasure,[1,2,3] Robert J. Siverd,[3] Michael C. Liu,[3] and Trent J. Dupuy[4]

[1] *Department of Earth, Atmospheric, and Planetary Sciences, Massachusetts Institute for Technology, 77 Massachusetts Avenue, Cambridge, MA 02139, USA*

[2] *Department of Physics, Massachusetts Institute for Technology, 77 Massachusetts Avenue, Cambridge, MA 02139, USA*

[3] *Institute for Astronomy, University of Hawai'i, 2680 Woodlawn Drive, Honolulu, HI 96822, USA*

[4] *Institute for Astronomy, University of Edinburgh, Royal Observatory, Blackford Hill, Edinburgh EH9 3HJ, UK*

ABSTRACT

We present a new distortion solution for the Canada-France-Hawaii Telescope's (CFHT) Wide-field InfraRed Camera (WIRCam) instrument. We imaged a calibration field centered around LHS3473 that contains roughly 2,000 stars in the H2 filter and roughly 5,000 stars in the J filter, many of which have Gaia astrometric measurements. By comparing the positions we measure with those in Gaia Lindegren et al. (2018), we determined the distortion solution of the WIRCam detector with precision on the subpixel level. We find the distortion solution has remained nearly constant over time and is very similar in the J and H2 filters. The distortion solution will eventually be released as part of a publicly available software package to compute parallax measurements from CFHT data (Siverd et al. in preparation).

Keywords: astronomy (804) — brown dwarfs — parallaxes — stars: distances — stars: low mass

1. INTRODUCTION

As the line between stars and planets, brown dwarfs set limits on the evolution processes of both. However, sophisticated models of brown dwarf evolution, such as Saumon & Marley (2008), do not accurately describe all observed brown dwarfs. For example, observations of low-gravity (VL-G) objects revealed that this model did not account for sufficiently red colors at a given absolute magnitude Best et al. (2015). Modelling these objects is difficult because they cool as they age and therefore have a degenerate relationship between mass, age, and luminosity. Thus, a young, low mass brown dwarf can have the same luminosity, temperature, and spectral type as an older, more massive brown dwarf. Further measurements of parallax distances, which are used to determine all three of mass, age, and luminosity, are needed to better constrain the models.

The Hawaii Infrared Parallax Program has made high-precision parallax measurements since 2007 (Dupuy & Liu (2012), Best et al. (2015), Dupuy et al. (2018), Best et al. (2020), and Zhang et al. (2021)). The CFHT WIRCam instrument has been used in this program and is sensitive to near-infared, 0.9-2.4 micron, wavelengths with a field of view of 20.5' x 20.5' Puget et al. (2004). WIRCam is made up of a grid of 4 HAWAII-2RG detectors that have a 45" gap between them, but only images from the northeast detector are used as part of the program since this detector has the least contamination. The CFHT has produced more abundant and higher precision parallax distances than other programs. As of 2016, the CFHT measured parallaxes of 115 ultracool objects with typical uncertainties of 1.3 mas. At the time, other programs, such as CTIO/BDKP (Faherty et al. (2012)), USNO IR (Vrba et al. (2004), Burgasser et al. (2008)), CTIOPI (Chabrier (2005), Costa et al. (2006), Henry et al. (2006), Gizis et al. (2007), Dieterich et al. (2014), Lurie et al. (2014), Riedel et al. (2014)) USNO CCD (Monet et al. (1992), Dahn et al. (2002), Dahn et al. (2008), Reid et al. (2003), Gizis et al. (2015)), and PARSEC (Andrei et al. (2011), Marocco et al. (2013)) have respectively measured the parallaxes of 70, 40, 60, 51, and 30 objects with typical errors of 6.9 mas, 3.8 mas, 1.7 mas, 1 mas, and 4 mas.

To further improve the precision of parallaxes from the CFHT, we computed a new distortion solution. Dupuy & Liu (2012) reported a distortion solution for WIRCam that used data taken from 2007 - 2010. All data was taken in the J filter and totaled 89 hours of queue scheduled observing. We imaged a calibration field centered around LHS3473, a high proper motion star, over the

course of 10 years. Data were collected using queue scheduled observing from 2011 to 2021 and 1,918 images were taken in total. Of these images, about half were 5-second exposures in the H2 filter and the other half were 20-second exposures in the J filter. To minimize atmospheric effects, all images were taken near the zenith, with a typical airmass of 1.05, and were dithered using CFHT's typical pattern. The larger data set taken over a longer time period enables us to compute a more robust distortion solution and evaluate its stability over time. In particular, more detected stars allows for better coverage on each pixel of the detector. Further, the distortion solution reported in Dupuy & Liu (2012) had residual rms values of about 40 mas which were dominated by positional errors in the reference star catalogs used, the Two Micron All Sky Survey (2MASS) Jarrett et al. (2000) and the Sloan Digital Sky Survey (SDSS) Ahn et al. (2021). We made use of the Gaia star catalog, which has typical astrometric uncertainties of 0.01 - 0.02 mas, 0.05 mas, and 0.4 mas for G<15, G=17, and G=20 respectively Lindegren et al. (2018). Additionally, data in both the J and H2 filter allow for the comparison of distortion across wavelengths. We find the distortion solution has remained nearly constant over time and is very similar in the J and H2 filters.

To measure the distortion solution, we computed astrometric positions of the stars in our data set and compared them to the values reported in Gaia. We used the World Coordinate System Greisen & Calabretta (2002) (WCS) convention and a tangent projection. This system is commonly used to relate the X and Y pixel coordinates in an image to sky RA and Dec. The WCS requires a CD matrix to translate the pixel coordinates into RA and Dec. In short, the CD matrix includes CD1_1, CD1_2, CD2_1, CD2_2, CRPIX1 and CRPIX2. CD1_1, CD1_2, CD2_1, and CD2_2 are a linear transformation matrix between the pixel axes and intermediate coordinate axes. CRPIX1 and CRPIX2 are the pixel values at the point of tangency which correspond to the RA and Dec coordinates CRVAL1 and CRVAL2. To find the best-fit WCS parameters we minimized the differences between our astrometric measurements and Gaia's. Once the match distances were minimized, we fit a 3rd polynomial to them as a function of location on the detector. In this paper, we describe the astrometric solution and matching to Gaia in section 2, the fitting of the distortion solution in section 3, and the stability of WIRCam over time in section 4.

2. ASTROMETRIC SOLUTION

2.1. *Data Acquisition and Source Extraction*

Calibrated ("p") WIRCam images were downloaded directly from the Canadian Astronomy Data Centre (CADC) using the astroquery Ginsburg et al. (2019) Cadc module and stored locally for processing. The Northeast sensor extension (HAWAII-2RG #60) was extracted from each image and stored separately, grouped by WIRCam run.

Each image was individually processed using custom Python software. Source extraction was perfomed using the SEP package Barbary (2016) which implements the algorithms of Source Extractor Bertin & Arnouts (1996). Sources were identified using a 2-sigma extraction threshold and detections covering at least 5 pixels were kept. Following this initial extraction, we performed a a row-by-row check for sources to identify horizontal detector artifacts. Rows containing more than 10 sources were flagged as unreliable and all associated measurements were dropped.

The resulting data set was used for the following astrometric analysis and distortion solution derivation. The routines described above are part of a forthcoming public software package for infrared parallax estimation (Siverd et al. in prep).

2.2. *Initial Astrometric Solution From 'I'iwi*

The data was preprocessed using 'I'iwi, the IDL Interpretor of WIRCam Images.[1] This pipeline calibrates the images and performs an initial astrometric fit using calibration stars from the 2MASS catalog. 'I'iwi performs source extraction using Source Extractor and then computes the WCS parameters. Using the detector geometry, 'I'iwi matches sources in the image to calibration stars in the 2MASS catalog. This fit first uses images from all four of WIRCam's detectors and then computes a more refined solution for each detector separately if enough sources are present. This astrometric solution is purely linear and the CD matrix values are reported in FITS header of each image. The number of sources used for the fit are also reported if there were enough stars for separate solutions for each of the four detectors. Only 22% of the images had enough sources for the by-detector fit, and in these cases 40 stars were typically used to compute the solution. The reported CD values in each image are used as the initial guess parameters for our astrometric solution. Histograms of the values of CD1_1, CD1_2, CD2_1, CD2_2 are shown in figure 1. As reported by 'I'iwi, the CD matrix values have little variation and have a standard deviation of $1.6e^{-7}$°, $2.2e^{-7}$°, $2.2e^{-7}$°, and $1.5e^{-7}$°respectively.

[1] https://www.cfht.hawaii.edu/Instruments/Imaging/WIRCam/IiwiVersion1Doc.html

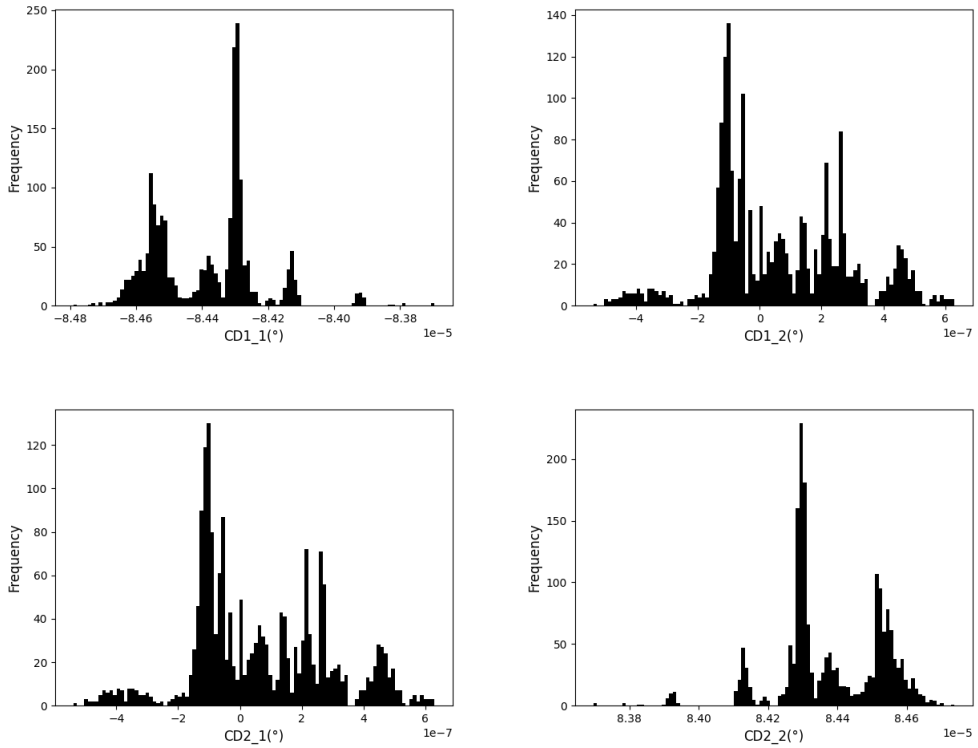

Figure 1. CD Matrix Values From the Image FITS Headers
These values are used as the initial guess parameters for solving for the best-fit CD matrix. Notice that there is little variation of the CD Matrix Values between the images and CD1_1, CD1_2, CD2_1, CD2_2 have a standard deviation of $1.6e^{-7}$°, $2.2e^{-7}$°, $2.2e^{-7}$°, and $1.5e^{-7}$°respectively.

2.3. *Matching to Gaia and Best-fit WCS Parameters*

The quality of the WCS parameters varies significantly across the sensor due to the presence of distortion. Match distance to Gaia across the detector using the initial WCS parameters from 'I'iwi is shown in figure 2. Near the center of the focal plane, the distortion is minimal. However, in the corners of the detectors farthest from the the center of the focal plane, stars are displaced by up to 5 arcseconds or 15 pixels. We needed to consider this distortion when matching stars to Gaia. The process of matching sources in the images to stars in the Gaia catalog required three steps. First, we identified preliminary matches using a modified nearest neighbor matching on each image individually. Secondly, we combined the matches from each image in order to perform outlier rejection across the data set. Thirdly, we reran the nearest neighbor matching on each image once more, using the matches from the first two steps and best-fit parameters from the FITS headers as the initial guesses. The output of the third step was the final Gaia matches and best-fit WCS parameters for each image. This output was used to create the distortion solution.

2.3.1. *Step 1: Modified Nearest Neighbor Matching*

The Gaia matching routine began with a nearest neighbor matching between the sources detected in an image and stars in the Gaia catalog. The WCS parameters included in the FITS header were used as the initial parameter guess. We started with a matching tolerance of 5 arcseconds as the maximum allowed distance between a source in our image and its corresponding Gaia match. These matches and best-fit parameters were used as the starting point for the following steps.

1. Iteration
   Once we had an initial match, we iterated over the best-fit parameters to improve the match until the parameters converged. Within each iteration, we took several other steps to improve the matching, namely outlier removal, match tolerance reduction, separation of the image into quadrants, and correction for proper motion. Each of these steps are described immediately below.

2. Outlier Removal
   Matches that had higher than typical errors were discarded. We only kept matches whose match distances was less than the 80th percentile since

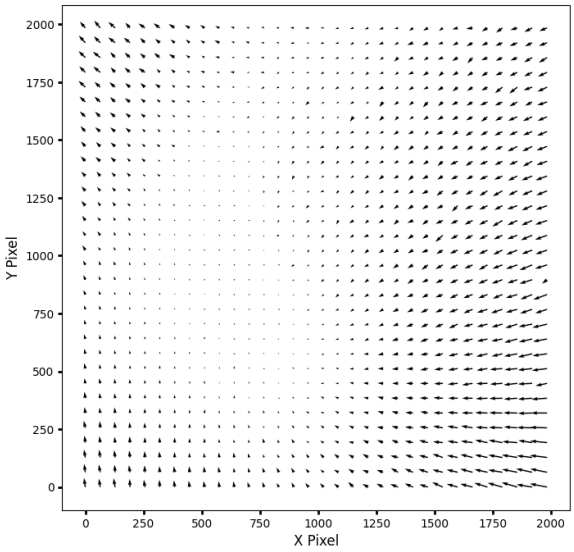

Figure 2. Match Distances Using WCS Parameters From 'I'iwi preprocessing pipeline.
The variation in the quality of the WCS parameters across the detector must be considered when performing matching to the Gaia catalog. In particular, matching can be improved by breaking the detector into quadrants and fitting different WCS parameters to each quadrant. After improving the matching by seperating each image into quadrants, we refit with a full-frame solution.

the distance as a function of percentile grew exponentially after this point.

The match distance as a function of percentile is displayed in figure 3.

3. Reduce Match Tolerance
   The initial fitting needs to use a tolerance of 5 arcseconds because this is the typical matching distance of the worst corner of the detector. However, this is much farther than is needed on the better portions of the detectors. After the global WCS is slightly improved, we re-detect matches with a tighter 2-arcsecond tolerance to reduce spurious matches and re-fit WCS. The difference between the measured RA and Dec and the values reported in Gaia is shown in figure 3. Be aware that figure 3 shows the match distance after step 2, but before step 3.

4. Separation Into Quadrants

   We divided each image into quadrants and ran the fitter on each quadrant separately. We noticed that the upper-left portion of the detector had the largest match distances. Since the error is non-uniform across the detector, discarding

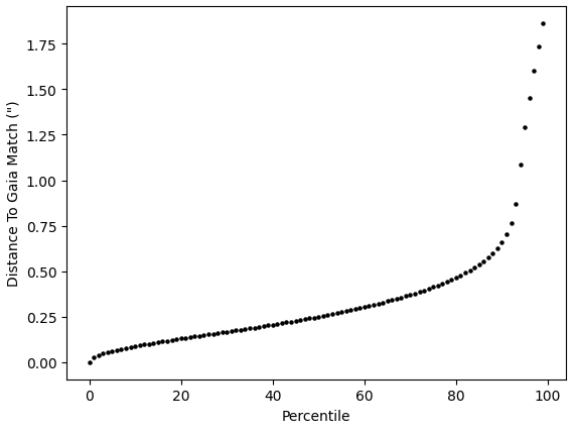

Figure 3. Match Distance Percentiles.
Matches with distances farther than the 80th percentile were removed from the best-fit solution because this function becomes exponential. Note that this plot represents intermediate Gaia matches after step 1, but before step 2 as described in section 3.2.

the most erroneous data points means discarding more points on some parts of the detector than others. Therefore, splitting the detector allows for outliers to be rejected more uniformly across the detector. Additionally, because a tangent projection was used for the astrometric fit, the best-fit WCS parameters were more accurate closer to the center of the solution. Therefore, splitting the image allows for different values of CRPIX1 and CRPIX2 in each quadrant.

5. Correction For Proper Motion
   Here, we update the positions of the Gaia stars to the time that observations were taken. This was done using the proper motions reported in the Gaia catalog. Although the median change in location due to proper motion was 0.074 pixels, there were about 50 sources matched to Gaia had a change of more than 0.5 pixels.

2.3.2. *Step 2: Outlier Rejection by Pixel Location*

We combined all of the Gaia matches from step 1 for another round of outlier removal. Even after tuning up the WCS to provide better across-the-frame results, the typical match error is a strong function of detector position due to distortion. Outlier rejection thus needs to be performed relative to the local separation distribution. The detector was divided into a 32x32 grid and each match was placed into the correct cell. Within each cell, we removed any match farther than 5σ away from the median match distance, either in RA or in Dec. This

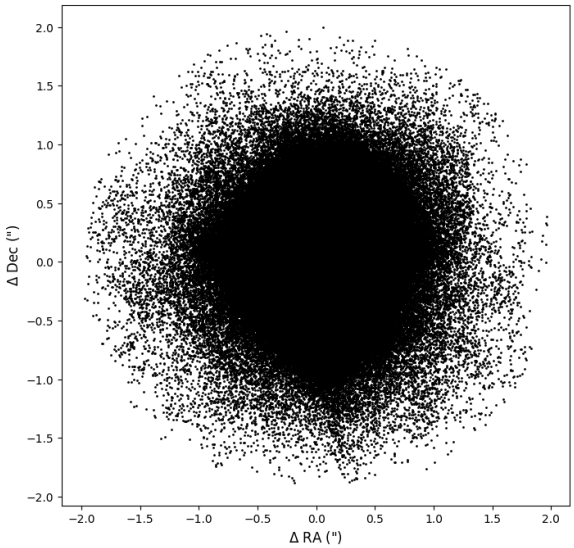

Figure 4. Distance Between Fitted Solution and Gaia Positions.
For a given match, here we show the difference between the RA and Dec of our astrometric solution and the value reported in the Gaia catalog. Again, note that this plot represents intermediate Gaia matches after step 2, but before step 3 as described in section 3.2.

is similar to the outlier removal in step 1. However, this round of outlier rejection differs from previous rounds due to the inclusion of data from many images.

2.3.3. *Step 3: Final Gaia Matching and Best-fit WCS Parameters*

Using the Gaia matches from step 2 and WCS parameters from the FITS headers as inputs, we ran refit the WCS parameters of each image a final time. At this stage, we did not use any of the features implemented in previous steps. The frequency of matches at each pixel location is reported in figure 4, and the relative distance of the match from Gaia as a function of pixel location is reported in figure 5. We were able to achieve even coverage of the detector and had about 1.8 million total Gaia matches. We also had even coverage at the subpixel level, as shown in figure 5. In general, there was a larger match distance farther from the center of the detector, with the top left corner having the most distortion. These WCS parameters and the distances at each detector location are directly used to compute the distortion polynomial.

2.4. *Wavelength Independence of Solution*

Since there could be chromatic aberration, wavelength dependent quantum efficiency, or other similar effects, we compared the WCS parameters of images in the H2 and J filters. We find the WCS parameters are very similar between the filters, so we do not compute separate distortion solutions for each filter.

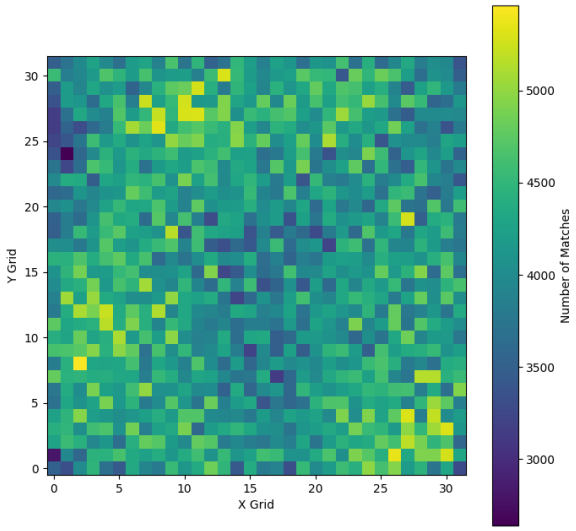

Figure 5. Frequency of Gaia Matches Across the Detector. The detector was split into a 32x32 grid and the number of matches of matches in each grid cell are displayed. Importantly, the matches evenly cover the entirety of the detector. This is the frequency of matches after all 3 steps have been completed, as described in section 3.2

3. DISTORTION SOLUTION

Using the best-fit WCS parameters, we fit a third order polynomial distortion solution for the detector. Dupuy & Liu (2012) found a 3rd order polynomial to be sufficient, so we adopt the same.

Essentially, we converted the match distances, as a function of X and Y pixel location on the detector, from RA and Dec to pixel units. Thus, we have one polynomial for the distortion in the X direction and another for the distortion in the Y direction. To solve for the best-fit coefficients, we performed a joint minimization of the pixel scale, coefficients, CRVAL1, and CRVAL2 useing the scipy Levenburg-Marqurat optimizaiton algorithm. We fit one pixel scale and set of coefficents across the entire data set, but calculate CRVAL1 and CRVAL2 for each image. Following the convention used in Dupuy & Liu (2012), we fixed CRPIX1 and CRPIX2 at -2122.6900 and 81.6789 respectively. We used the 2012 distortion solution and CRVAL1 and CRVAL2 from the WCS parameters computed in step 3 as the initial guess for this optimization. We found that this minimization would take on the order of compute-months to run on the entire data set. As a result, we performed ran the optimizer twice, once on the first 250 images in the data set and once on the last 250 images in the data set. These two minimizations resulted in very similar

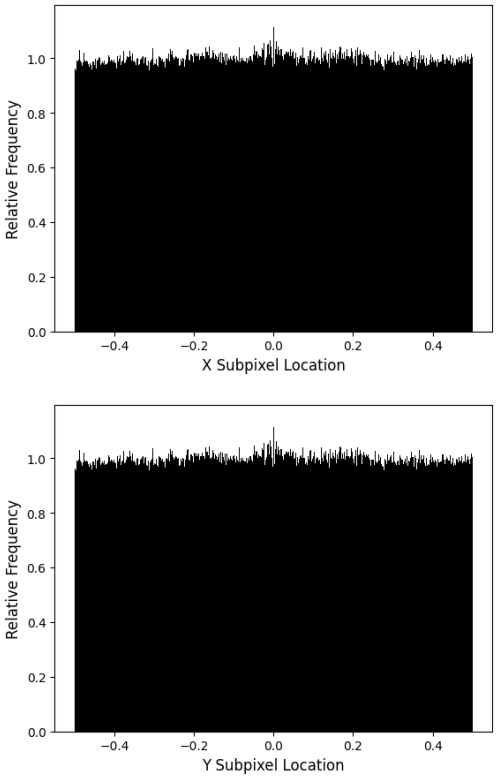

Figure 6. Subpixel Locations of Gaia Matches.
The subpixel locations of the matches are evenly sampled in both the X and Y directions. This indicates that each pixel is uniformly sensitive.

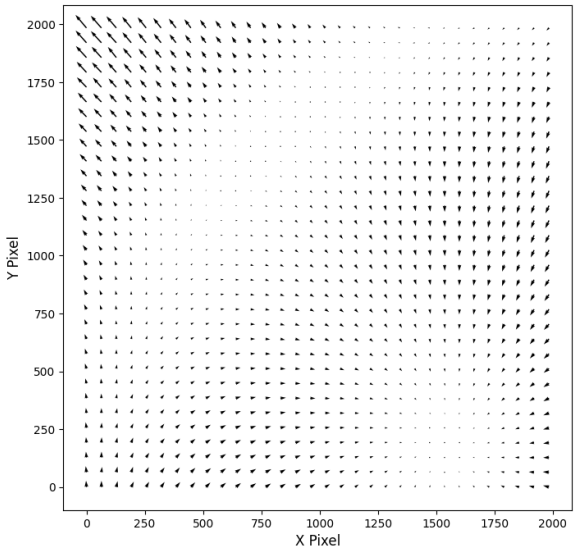

Figure 7. Match Distance Across The Detector
This displays the distance between the calculated RA and Dec of every source in the CFHT data with its corresponding match in the Gaia catalog. For display purposes, we imposed a 32x32 grid on the detector and computed the median distance within each grid cell. For scale, the longest arrow represents 2.20 arcseconds. Each arrow represents the median distance of the matches within a grid cell. These distances are computed after all 3 steps described in section 3.2 have been completed.

distortion solutions, but had slightly different residuals. In both cases, the residuals of the distortion solution are on the subpixel level. This distortion coefficents are reported in table 1 and the residuals are shown in figure 10. In the future, we plan to use an Markov chain Monte Carlo fitter to perform this optimization across the entire data set.

4. STABILITY OF WIRCAM OVER TIME

Since we have data collected from 2011-2021 in addition to the distortion solution presented in Dupuy & Liu (2012) we can evaluate the stability of the detector over time. Notably, WIRCam is taken on/off of the telescope about 8 times per year, when there is a new observing run. This has the potential to change the distortion parameters. We find that the orientation of the detector has 0.4° variation over the 10 year period, but that the X and Y pixel scales are constant. We also find that our distortion solution is consistent with the one reported in Dupuy & Liu (2012).

5. FUTURE WORK

This work is inspired by a data analysis pipeline which measures brown dwarf parallaxes from Spitzer

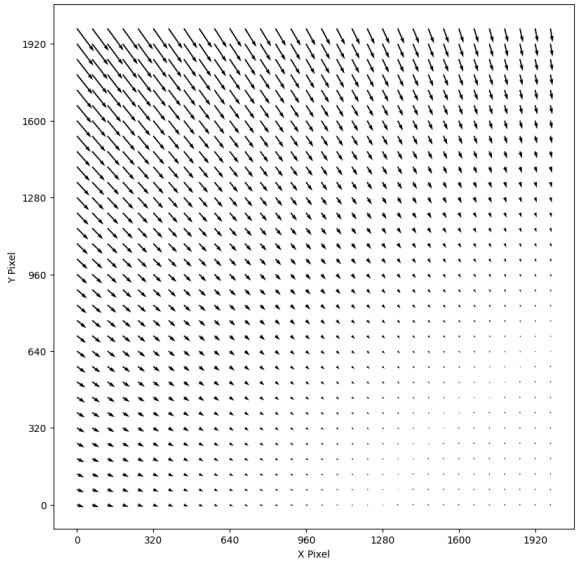

Figure 8. Distortion Solution in The Northeast array of the WIRCam Mosaic
The distortion increases radially outward, away from the center of the mosaic. The distortion solution is consistent with the one presented in Dupuy & Liu (2012). This plot is a visual representation of the distortion polynomial presented in table 1.

Term	$\alpha\ a_{ij}$	$\beta\ a_{ij}$	2012 a_{ij}	$\alpha\ b_{ij}$	$\beta\ b_{ij}$	2012 b_{ij}
x^2	1.17e^{-6}	1.17e^{-6}	1.73e^{-6}	-6.41e^{-7}	-6.41e^{-7}	-6.409e^{-7}
xy	-1.30e^{-6}	-1.30e^{-6}	-1.303e^{-6}	1.12e^{-6}	1.12e^{-6}	1.117e^{-6}
y^2	5.10e^{-7}	5.10e^{-7}	5.105e^{-7}	-1.19e^{-6}	-1.19e^{-6}	-1.191e^{-6}
x^3	-5.29e^{-10}	-5.29e^{-10}	-5.287e^{-10}	-1.47e^{-10}	-1.47e^{-10}	-1.466e^{-10}
x^{2y}	-4.13e^{-10}	-4.13e^{-10}	-4.130e^{-10}	-4.59e^{-10}	-4.59e^{-10}	-4.589e^{-10}
xy^2	-5.34e^{-10}	-5.34e^{-10}	-5.338e^{-10}	-3.88e^{-10}	-3.88e^{-10}	-3.884e^{-10}
y^3	-1.35e^{-10}	-1.35e^{-10}	-1.353e^{-10}	-5.87e^{-10}	-5.87e^{-10}	-5.872e^{-10}

Table 1. Distortion Coefficients for WIRCam Northeast Array
As described in section 3, we computed two different sets of polynomials with different subsets of the data. The coefficients labeled with α correspond to the first 250 images and the coefficients labeled with β correspond to the last 250 images. To apply this polynomial, the origin should be defined using CRPIX1 and CRPIX2.

data (Siverd et al. in prep). This distortion solution will become part of a publicly available, self-consistent multi-observatory parallax measurement pipeline. Using this pipeline, we will recompute parallax measurements of previous Hawaii Infrared Parallax program CFHT targets. This distortion solution will not only allow for higher-precision parallax measurements, but will aid the search for new ultracool objects, astrometric perturbations, and associations with moving groups.

1. Abigail Colclasure acknowledges support from Research Experience for Undergraduate program at the Institute for Astronomy, University of Hawaii-Manoa funded through NSF grant #2050710.

2. Abigail Colclasure would like to thank the Institute for Astronomy for their hospitality during the course of this project.

3. This work is based on observations made by CFHT. We wish to extend our special thanks to those of Hawaiian ancestry on whose sacred mountain of Maunakea we are privileged to be guests. The observations presented herein would not have been possible without their generosity.

4. This work has made use of data from the European Space Agency (ESA) mission *Gaia* (https://www.cosmos.esa.int/gaia), processed by the *Gaia* Data Processing and Analysis Consortium (DPAC, https://www.cosmos.esa.int/web/gaia/dpac/consortium). Funding for the DPAC has been provided by national institutions, in particular the institutions participating in the *Gaia* Multilateral Agreement.

5. This work made use of Astropy:[2] a community-developed core Python package and an ecosystem of tools and resources for astronomy (Astropy Collaboration et al. 2013, 2018; **?**).

REFERENCES

Ahn, C. P., Alexandroff, R., Allende Prieto, C., et al. 2021, arXiv e-prints. https://arxiv.org/abs/2105.13597

Andrei, A. H., Smart, R. L., Penna, J. L., et al. 2011, AJ, 141, 54, doi: 10.1088/0004-6256/141/2/54

Astropy Collaboration, Robitaille, T. P., Tollerud, E. J., et al. 2013, A&A, 558, A33, doi: 10.1051/0004-6361/201322068

Astropy Collaboration, Price-Whelan, A. M., Sipőcz, B. M., et al. 2018, AJ, 156, 123, doi: 10.3847/1538-3881/aabc4f

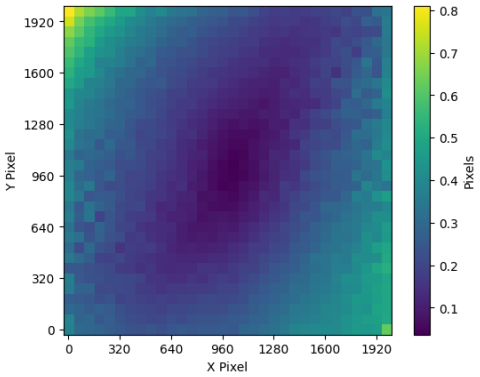

Figure 9. Residual using the distoriton solution generated with the first 250 images.

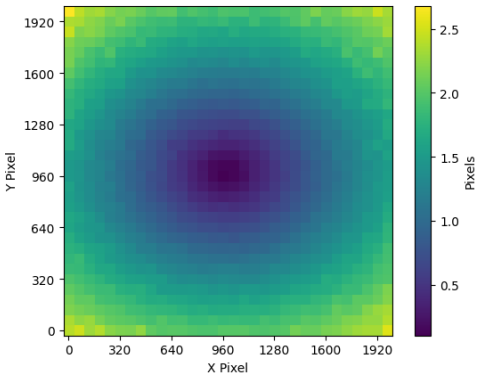

Figure 10. Residual using the distortion solution generated with the last 250 images.

Figure 11. Residual Match Distances After Model Fit
After applying the distortion solution, the match distances are on the subpixel level. This is a great improvement from the as much as 15 pixel error associated with the astrometric fits from the 'I'iwi preprocessing pipeline. To solve for the best-fit coefficients, we performed a joint minimization of the pixel scale, coefficients, CRVAL1, and CRVAL2 using the scipy Levenburg-Marqurat optimization algorithm as described in section 3. We found that this minimization would take on the order of compute-months to run on the entire data set. As a result, we performed ran the optimizer twice, once on the first 250 images in the data set and once on the last 250 images in the data set. These two minimisations resulted in very similar distortion solutions, but had slightly different residuals. In the future, we plan to use an MCMC fitter to perform this optimization across the entire data set.

Barbary, K. 2016, Journal of Open Source Software, 1, 58, doi: 10.21105/joss.00058

Bertin, E., & Arnouts, S. 1996, A&AS, 117, 393, doi: 10.1051/aas:1996164

Best, W. M. J., Liu, M. C., Magnier, E. A., & Dupuy, T. J. 2020, AJ, 159, 257, doi: 10.3847/1538-3881/ab84f4

Best, W. M. J., Liu, M. C., Magnier, E. A., et al. 2015, ApJ, 814, 118, doi: 10.1088/0004-637X/814/2/118

Burgasser, A. J., Vrba, F. J., Lépine, S., et al. 2008, ApJ, 672, 1159, doi: 10.1086/523810

Chabrier, G. 2005, in Astrophysics and Space Science Library, Vol. 327, The Initial Mass Function 50 Years Later, ed. E. Corbelli, F. Palla, & H. Zinnecker, 41, doi: 10.1007/978-1-4020-3407-7_5

Costa, E., Méndez, R. A., Jao, W. C., et al. 2006, AJ, 132, 1234, doi: 10.1086/505706

Dahn, C. C., Harris, H. C., Vrba, F. J., et al. 2002, AJ, 124, 1170, doi: 10.1086/341646

Dahn, C. C., Harris, H. C., Levine, S. E., et al. 2008, ApJ, 686, 548, doi: 10.1086/591050

Dieterich, S. B., Henry, T. J., Jao, W.-C., et al. 2014, AJ, 147, 94, doi: 10.1088/0004-6256/147/5/94

Dupuy, T. J., & Liu, M. C. 2012, ApJS, 201, 19, doi: 10.1088/0067-0049/201/2/19

Dupuy, T. J., Liu, M. C., Allers, K. N., et al. 2018, AJ, 156, 57, doi: 10.3847/1538-3881/aacbc2

Faherty, J. K., Burgasser, A. J., Walter, F. M., et al. 2012, ApJ, 752, 56, doi: 10.1088/0004-637X/752/1/56

Ginsburg, A., Sipőcz, B. M., Brasseur, C. E., et al. 2019, AJ, 157, 98, doi: 10.3847/1538-3881/aafc33

Gizis, J. E., Allers, K. N., Liu, M. C., et al. 2015, ApJ, 799, 203, doi: 10.1088/0004-637X/799/2/203

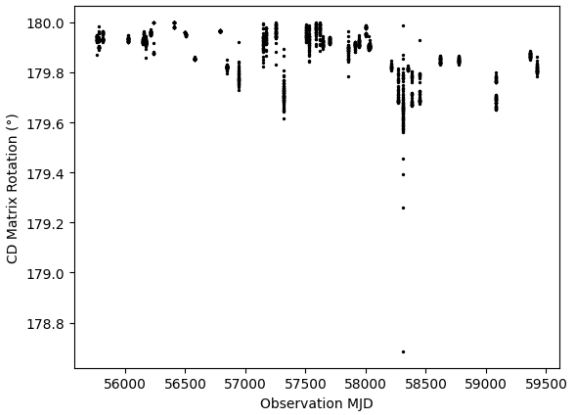

Figure 12. CD Matrix Rotation Over Time
There is about 0.4° of variation in the orientation of WIRCam from 2011-2021. This is likely the result of WIRCam being taken on/off of the telescope 8 times per year, when there is a new observing run

Gizis, J. E., Jao, W.-C., Subasavage, J. P., & Henry, T. J. 2007, ApJL, 669, L45, doi: 10.1086/523271

Greisen, E. W., & Calabretta, M. R. 2002, A&A, 395, 1061, doi: 10.1051/0004-6361:20021326

Henry, T. J., Jao, W.-C., Subasavage, J. P., et al. 2006, AJ, 132, 2360, doi: 10.1086/508233

Jarrett, T. H., Chester, T., Cutri, R., et al. 2000, The Astronomical Journal, 119, 2498, doi: 10.1086/301330

Lindegren, L., Hernández, J., Bombrun, A., et al. 2018, A&A, 616, A2, doi: 10.1051/0004-6361/201832727

Lurie, J. C., Henry, T. J., Jao, W.-C., et al. 2014, AJ, 148, 91, doi: 10.1088/0004-6256/148/5/91

Marocco, F., Andrei, A. H., Smart, R. L., et al. 2013, AJ, 146, 161, doi: 10.1088/0004-6256/146/6/161

Monet, D. G., Dahn, C. C., Vrba, F. J., et al. 1992, AJ, 103, 638, doi: 10.1086/116091

Puget, P., Stadler, E., Doyon, R., et al. 2004, in Society of Photo-Optical Instrumentation Engineers (SPIE) Conference Series, Vol. 5492, Ground-based Instrumentation for Astronomy, ed. A. F. M. Moorwood & M. Iye, 978–987, doi: 10.1117/12.551097

Reid, I. N., Cruz, K. L., Laurie, S. P., et al. 2003, AJ, 125, 354, doi: 10.1086/344946

Riedel, A. R., Finch, C. T., Henry, T. J., et al. 2014, AJ, 147, 85, doi: 10.1088/0004-6256/147/4/85

Saumon, D., & Marley, M. S. 2008, ApJ, 689, 1327, doi: 10.1086/592734

Vrba, F. J., Henden, A. A., Luginbuhl, C. B., et al. 2004, AJ, 127, 2948, doi: 10.1086/383554

Zhang, Z., Liu, M. C., Best, W. M. J., Dupuy, T. J., & Siverd, R. J. 2021, ApJ, 911, 7, doi: 10.3847/1538-4357/abe3fa

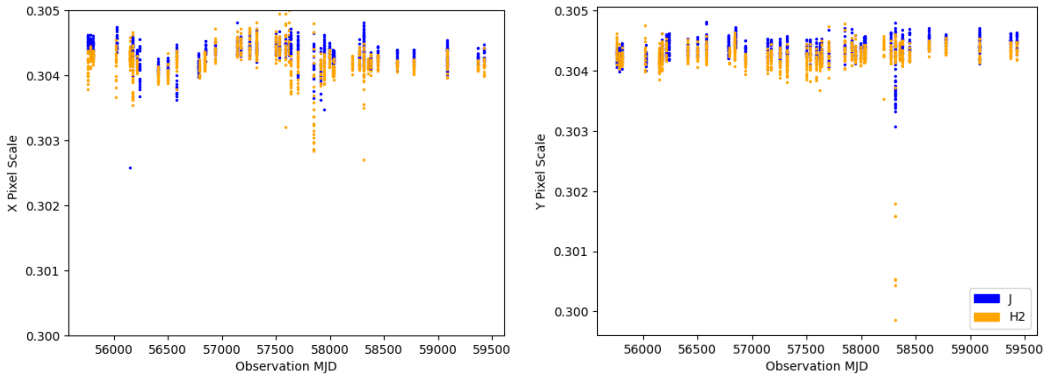

Figure 13. Pixel Scales of the X and Y Axes Over Time
The pixel scale is stable over time and the ratio of the x and y pixel scales is consistent with unity. The pixel scales are consistent between the H2 and J filters.